Role of Protein Phosphatase1 Regulatory Subunit3 in Mediating the Abscisic Acid Response[1][OPEN]

Jing Zhang,[a,2] Qianqian Qin,[a,2] Xiaohui Nan,[a] Zilong Guo,[b] Yang Liu,[a] Sawaira Jadoon,[a] Yan Chen,[a] Lulu Zhao,[a] Longfeng Yan,[a] and Suiwen Hou[a,3,4]

[a]Ministry of Education Key Laboratory of Cell Activities and Stress Adaptations, School of Life Sciences, Lanzhou University, Lanzhou 730000, China

[b]Root Biology Center, Fujian Agriculture and Forestry University, Fuzhou 350002, China

ORCID ID: 0000-0003-1961-4216 (S.H.).

Protein phosphatase1 (PP1) plays important roles in eukaryotes, including in plant hormone responses, and functions as a holoenzyme that consists of catalytic and regulatory subunits. Animal genomes encode ~200 PP1-interacting proteins; by contrast, only a few have been reported in plants. In this study, PP1 Regulatory Subunit3 (PP1R3), a protein that interacts with PP1 in Arabidopsis (*Arabidopsis thaliana*), was characterized by mass spectrometry. *PP1R3* was widely expressed in various plant tissues and PP1R3 colocalized with Type One Protein Phosphatases (TOPPs) in the nucleus and cytoplasm. The *pp1r3* mutants were hypersensitive to abscisic acid (ABA), similar to the dominant-negative mutant *topp4-1* or the loss-of-function multiple mutants *topp1 topp4-3*, *topp8 topp9*, *topp6/7/9*, *topp1/2/4-3/6/7/9*, and *topp1/4-3/5/6/7/8/9* (*topp-7m*). About two-thirds of differentially expressed genes in *topp-7m* showed the same gene expression changes as in *pp1r3-2*. In response to ABA, the phenotypes of *pp1r3 topp1 topp4-3* and *pp1r3 topp4-1* were consistent with those of *pp1r3*, while *pp1r3 abi1-1* showed an additive effect of the *pp1r3* and *abi1-1* (mutation in *Abscisic Acid Insensitive1* [*ABI1*]) single mutants. Moreover, *pp1r3* could partially recover the ABA response-related phenotype, gene expression, and plant morphology of *topp4-1*. PP1R3 inhibited TOPP enzyme activity and facilitated the nuclear localization of TOPP4. By contrast, ABA treatment increased the amounts of TOPP1 and TOPP4 in the cytoplasm. Importantly, nuclear localization of TOPP4 partially restored the ABA-hypersensitive phenotype of *topp4-1*. Overall, our results suggest that the PP1R3:TOPP holoenzyme functions in parallel with ABI1 in the nucleus to regulate ABA signaling.

Under adverse environmental conditions, such as water deficiency, high salinity, or abnormal temperature, plants activate stress response mechanisms to increase their chances of survival (Zhu, 2016). The phytohormone abscisic acid (ABA) is pivotal to stress responses and plant development, affecting processes such as seed maturation, seed germination, and aging (Finkelstein, 2013; Vishwakarma et al., 2017). Plants increase ABA levels under adverse conditions in a number of ways. For example, when activated by drought, the rice (*Oryza sativa*) kinase Stress-Activated Protein Kinase2 (SAPK2) promotes the transcriptional activity of Basic Leu Zipper23 (OsbZIP23) by phosphorylation. This promotes the expression of *9-cis-Epoxycarotenoid Dioxygenase4* (*OsNCED4*), a key gene for ABA synthesis, which increases ABA concentration (Zong et al., 2016). ABA 8′-hydroxylases (CYP707As) catalyze the first committed step in the predominant ABA catabolic pathway, and overexpression of the maize (*Zea mays*) E3 ubiquitin ligase genes *ZmXerico1* and *ZmXerico2* induce degradation of CYP707As, enhancing plant drought tolerance (Brugière et al., 2017). The core ABA signaling pathway consists of Pyrabactin-Resistance (PYR)/PYR1-Like (PYL)/Regulatory Components of ABA Receptor (RCAR) receptors, clade A type 2C protein phosphatases (PP2CAs), Suc Nonfermenting-1-Related Protein Kinase2s (SnRK2s), and substrates of SnRK2s, including membrane proteins, transcription factors, and other proteins (Finkelstein, 2013; Hauser et al., 2017). The regulation of ABA signaling is a precise and complex process involving several post-translational protein modifications, including phosphorylation, ubiquitination, and nitrosylation. Protein

[1]This work was supported by the Ministry of Agriculture of the People's Republic of China (grant no. 2016ZX08009–003–002), the National Natural Science Foundation of China (grant nos. 31870251, 31470372, and 31600156), the Major Project of Science and Technology of Gansu Province (grant no. 17ZD2NA016), the Chang Jiang Scholars Program of China, and Fundamental Research Funds for the Central Universities (grant nos. lzujbky–2015–226 and lzujbky–2018–106).

[2]These authors contributed equally to the article.

[3]Author for contact: housw@lzu.edu.cn.

[4]Senior author.

The author responsible for distribution of materials integral to the findings presented in this article in accordance with the policy described in the Instructions for Authors (www.plantphysiol.org) is: Suiwen Hou (housw@lzu.edu.cn).

J.Z. and S.W.H designed the experiments and wrote the manuscript; J.Z., Q.Q.Q., X.H.N., Y.L., C.Y., and L.L.Z. performed the experiments; J.Z., Q.Q.Q., S.J., and S.W.H. revised the manuscript; Q.Q.Q., L.F.Y., and Z.L.G. performed the RNA-Seq data analysis.

[OPEN]Articles can be viewed without a subscription.

www.plantphysiol.org/cgi/doi/10.1104/pp.20.01018

phosphorylation functions as an on/off switch in the ABA signaling pathway (Yu et al., 2016; Yang et al., 2017; Zhang et al., 2019).

Phosphorylation, a reversible posttranslational modification that regulates protein function and biological processes, is carried out by protein kinases and reversed by protein phosphatases (Humphrey et al., 2015). In eukaryotes, protein phosphatase1 (PP1) is a major member of the Ser/Thr phosphoprotein phosphatase family that dephosphorylates most phosphoproteins (Shi, 2009). PP1 is widely distributed in eukaryotes and is involved in glycogen metabolism, mitosis, circadian rhythm, and other important cellular processes in animals (Ceulemans and Bollen, 2004; Fang et al., 2007; Kamimura et al., 2015). The PP1 holoenzyme consists of a conserved catalytic subunit (PP1c) and diverse regulatory subunits (PP1rs). Most PP1rs have intrinsically disordered regions (IDRs) including RVxF and SILK motifs, for substrate recruitment, PP1 inhibition, and subcellular targeting (Bollen et al., 2010; Verbinnen et al., 2017). More than 70% of PP1rs contain an RVxF motif. However, some PP1rs lack this motif, including fission yeast (*Schizosaccharomyces pombe*) Suppressor of $dis2^+$ (SDS22), which is a representative atypical PP1r (Ohkura and Yanagida, 1991). Although SDS22 is a Leu-rich repeat protein without IDRs, it contains multiple tandem parallel β-sheets essential for binding to PP1c (Ceulemans et al., 2002; Choy et al., 2018). Furthermore, SDS22 can interact with a typical PP1r, such as Inhibitor-3 (INH3), to form an INH3:SDS22:PP1 ternary complex (Pedelini et al., 2007; Eiteneuer et al., 2014). PP1rs compete with each other and dynamically bind to PP1c in different cellular compartments, which is the basis for precise regulation of PP1 in specific physiological processes (Heroes et al., 2013).

Although the role of PP1 in animals is well understood, few reports have examined the functions of PP1s in plants. *PP1 Regulatory Subunit2-Like Protein1* (*PRSL1*), a homolog of *Vicia faba VfPRS2*, participates in blue light-mediated stomatal movement in Arabidopsis (*Arabidopsis thaliana*; Takemiya et al., 2013). Potato (*Solanum tuberosum*) StPP1c interacts with the *Phytophthora infestans* effector Pi04314 to regulate late blight disease (Boevink et al., 2016). A recent study reported that *Type One Protein Phosphatase9* (*TOPP9*)/*ATUNIS1* (*AUN1*) and *TOPP8/AUN2* regulate cell wall integrity during tip growth, affecting pollen tube and root hair growth in Arabidopsis (Franck et al., 2018). Similarly, a few PP1rs of TOPPs (TOPP1 to TOPP9 in the Arabidopsis PP1 family) have been identified thus far, including INH3, PRSL1, and AtInhibitor-2 (AtI-2; Takemiya et al., 2009, 2013; Templeton et al., 2011). AtINH3, the first reported PP1r in Arabidopsis and a homolog of human (*Homo sapiens*) INH3, regulates PP1 activity and nuclear localization of PP1c and is essential for embryogenesis (Takemiya et al., 2009). AtI-2, a homolog of the ancient regulatory subunit I-2, contains a conserved RVxF motif and inhibits the activity of TOPPs (Templeton et al., 2011). A subsequent study reported that the TOPP1:AtI-2 holoenzyme regulates ABA response by inhibiting the kinase activity of SnRK2.6 (Hou et al., 2016).

Previously, we identified and used a dominant-negative mutant of *TOPP4*, *topp4-1*, to show that TOPP4 participates in DELLA-mediated GA signaling, Pin-Formed1 (PIN1)-mediated pavement cell morphogenesis, and Phytochrome Interacting Factor5 (PIF5)-regulated light morphogenesis by dephosphorylating different substrates (Qin et al., 2014; Guo et al., 2015; Yue et al., 2016). Recently, we found that TOPPs interact with Suppressor of *topp4-1* (SUT1), a coiled-coil-nucleotide-binding site-Leu-rich-repeat resistance protein that contributes to plant immunity (Yan et al., 2019; Liu et al., 2020). However, detailed investigation reveals that understanding TOPPs and their substrate relationships does not fully explain how TOPPs regulate specific cell processes. Here, to better understand the physiological function of TOPPs in Arabidopsis, we performed affinity purification of the TOPP4-GFP fusion protein and identified the regulatory subunits of TOPPs using mass spectrometry. We identified a TOPP-interacting protein named PP1 Regulatory Subunit3 (PP1R3) that regulated TOPP phosphatase activity and nuclear localization. Compared with wild-type (ecotype Columbia [Col-0] of Arabidopsis), two *pp1r3* T-DNA insertion mutants were more sensitive to ABA and salinity, similar to *topp* mutants. Genetic analysis showed that PP1R3 and TOPPs jointly regulate the ABA response, and that regulation of TOPP4 subcellular localization is important for TOPP-mediated ABA signaling.

RESULTS

Copurification of TOPP4 Protein Complex Components

To search for TOPP interactors, TOPP4 was fused to GFP and expressed under control of the constitutive *Cauliflower mosaic virus* 35S promoter. Overexpression of *TOPP4-GFP* partially rescued the phenotypes of the *topp4-1* dominant negative mutant (Fig. 1A), consistent with overexpression of *TOPP4* (Qin et al., 2014; Guo et al., 2015), verifying that the *TOPP4-GFP* fusion gene was functionally identical to *TOPP4.* As a control, overexpression of *GFP* did not affect the phenotype of *topp4-1* (Fig. 1A). Immunoblotting using an anti-GFP antibody detected the accumulation of TOPP4-GFP and GFP proteins in the respective transgenic lines (Fig. 1B). The results indicated that the TOPP4-GFP fusion protein was functional in planta.

When the proteins purified using an anti-GFP antibody were separated by SDS-PAGE, Coomassie blue staining detected some specific bands from TOPP4-GFP copurified proteins (Fig. 1C). Using mass spectroscopy, we found an increase in unique peptides, including TOPP4, the TOPP-interacting protein AtINH3 (Takemiya et al., 2009), and PP1R3 among the coprecipitates of TOPP4-GFP, compared with those of GFP (Table 1; Supplemental Table S1). To verify whether these proteins

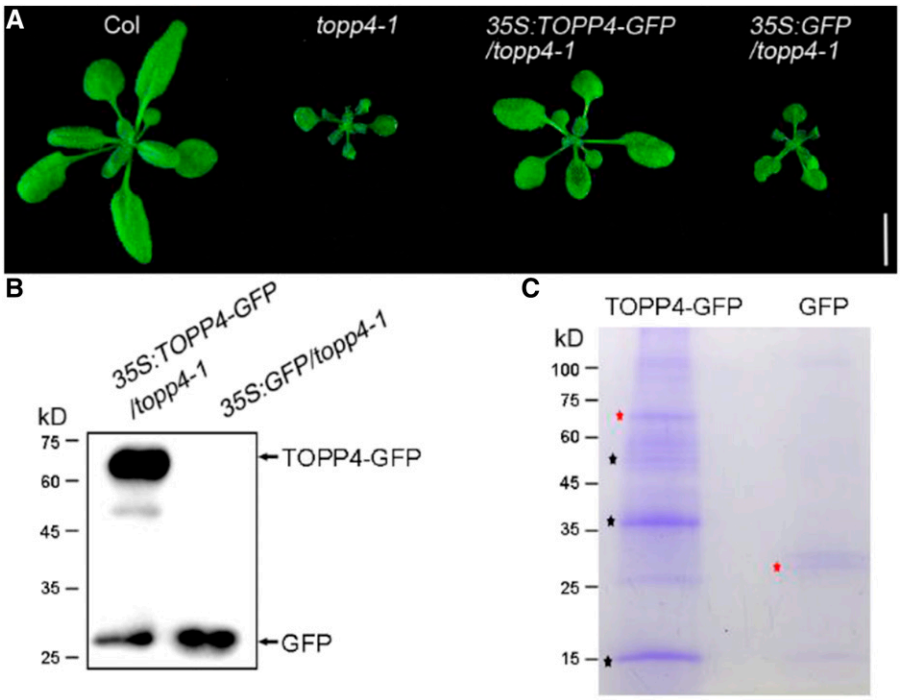

Figure 1. Purification and separation of the coprecipitates of TOPP4-GFP. A, Phenotypes of 3-week-old plants. Scale bar = 1 cm. B, Detection of TOPP4-GFP and GFP protein accumulation. Anti-GFP antibody was used for western blotting. The scale on the left indicates the molecular mass of the protein. C, Isolation of coprecipitates by SDS-PAGE and Coomassie blue staining. Red asterisks indicate TOPP4-GFP or GFP protein and black asterisks indicate TOPP4-GFP-specific bands.

interacted directly with TOPP4, we selected some for confirmation by yeast two-hybrid (Y2H) experiments. Several proteins, including PP1R3, interacted with TOPP4, whereas some proteins did not (Table 1). Therefore, PP1R3 was selected for further study.

PP1R3 Physically Interacts with TOPPs

As shown in Figure 2A, PP1R3 showed a strong interaction with TOPP4 in the Y2H system. To confirm the interaction of TOPP4 with PP1R3 in vivo, we performed coimmunoprecipitation (Co-IP) and bimolecular fluorescence complementation (BiFC) assays. For the Co-IP assay, we constructed fusion genes containing FLAG tag (peptide DYKDDDDK) or HA tag (peptide YPYDVPDYA). *PP1R3-FLAG* was coexpressed in *Nicotiana benthamiana* epidermal cells with *TOPP4-HA* or *Red Fluorescent Protein* (*RFP*)*-HA*. We found that PP1R3 coprecipitated with TOPP4 but not with RFP (Fig. 2B). For the BiFC assays, PP1R3 was fused to the C-terminal fragment of yellow fluorescent protein (YFP; PP1R3-YC) and TOPP4 was fused to the N-terminal fragment of YFP (TOPP4-YN). Strong YFP fluorescence was observed in both the nucleus and cytoplasm of epidermal cells when *PP1R3-YC* and *TOPP4-YN* were coexpressed in *N. benthamiana* leaves (Fig. 2C). Weak YFP fluorescence was observed in control cells coexpressing *PP1R3-YC* and *SnRK1.1-YN*, whereas no fluorescence was observed in cells coexpressing *TOPP4-YN* and the Arabidopsis homolog of yeast, *Protein Associated with Topoisomerase II* (*PAT1*)*-YC* (Fig. 2C).

Using the Y2H assay, we tested whether the other TOPPs could interact with PP1R3. As expected, except for TOPP3, which bound weakly to PP1R3, the other eight TOPPs strongly interacted with PP1R3 in vitro (Fig. 2A). Moreover, PP1R3 interacted with topp4-1, the mutant protein produced by the *topp4-1* dominant negative allele (Fig. 2A).

Our protein sequence analysis showed that PP1R3 was homologous to SDS22 in fission yeast (Supplemental Fig. S1A). The C-terminal cap domain of SDS22 is critical for interacting with PP1c (Pedelini et al., 2007). To test the interaction of the PP1R3 C-terminal cap with TOPPs, we constructed a truncated form of PP1R3 (PP1R3ΔC) that lacks the C-terminal domain (Supplemental Fig. S1B). The results showed weak interactions between PP1R3ΔC and TOPPs (Supplemental Fig. S1C), indicating that the C terminus of PP1R3 was important for its interaction with TOPPs. We also mapped regions of TOPP4 involved in interaction with PP1R3 (Supplemental Fig. S1B). The large truncations at the C terminus (ΔC88 and ΔC169) slightly attenuated the interaction of TOPP4 with PP1R3, but N-terminal truncations of TOPP4 (ΔN56 and ΔN153) completely inhibited the interaction (Supplemental Fig. S1D), indicating that the TOPP4-PP1R3 interaction depended on the N terminus of TOPP4. These results indicated that PP1R3 is a TOPP-interacting protein in Arabidopsis.

Subcellular Localization of PP1R3 and Expression Patterns of *PP1R3*

Because PP1R3 and TOPPs interacted in Y2H assays, we hypothesized that they colocalized in vivo. As expected, after coexpressing *PP1R3-RFP* and *TOPP4-GFP* in *N. benthamiana* leaves, we observed PP1R3-RFP in the

Table 1. *TOPP4-GFP copurification proteins and Y2H confirmation*

Dashes indicate that no peptides were detected in the sample by mass spectrometry. Interaction between the bait and prey proteins was confirmed as strong (Y) or weak (W) or was not detected (N). PP1R1 to PP1R3, putative PP1 regulatory subunits in Arabidopsis.

Gene	Protein	TOPP4-GFP		GFP		Confirmation
		Unique Peptides	Coverage	Unique Peptides	Coverage	
		No.	*%*	*No.*	*%*	
AT2G39840	TOPP4	20	74.8	2	7.4	Y
AT1G50600	SCL5	1	1.34	2	2	W
At3G18060	PP1R1	1	1.67	2	2	N
AT5G14530	PP1R2	5	18.48	2	2	W
AT5G03280	EIN2	1	0.54	—	—	N
AT4G09000	GRF1	9	31.3	4	20.2	W
AT5G16050	GRF5	5	18	6	26	Y
AT2G31305	AtINH3	2	31.5	—	—	Y
AT5G19680	PP1R3	14	56.4	1	3.6	Y
AT5G63020	Disease resistance protein/SUT1	1	2.61	—	—	Y
At5G56030	HSP90-2	5	8	4	7.5	W
AT3G45640	MPK3	2	10	2	8.9	Y
AT2G43790	MPK6	—	—	—	—	Y

nucleus and cytoplasm, where it colocalized with TOPP4-GFP (Fig. 3A). Furthermore, PP1R3 also localized in the cytoplasm and nucleus, as shown using transient expression assays in Arabidopsis protoplasts (Fig. 3B), and the subcellular localization of PP1R3 was similar to that reported for TOPPs (Takemiya et al., 2009; Qin et al., 2014; Guo et al., 2015).

To determine the expression pattern of *PP1R3*, we constructed transgenic plants expressing a *PP1R3* native promoter (~1.8 kb) driving the *PP1R3* genomic

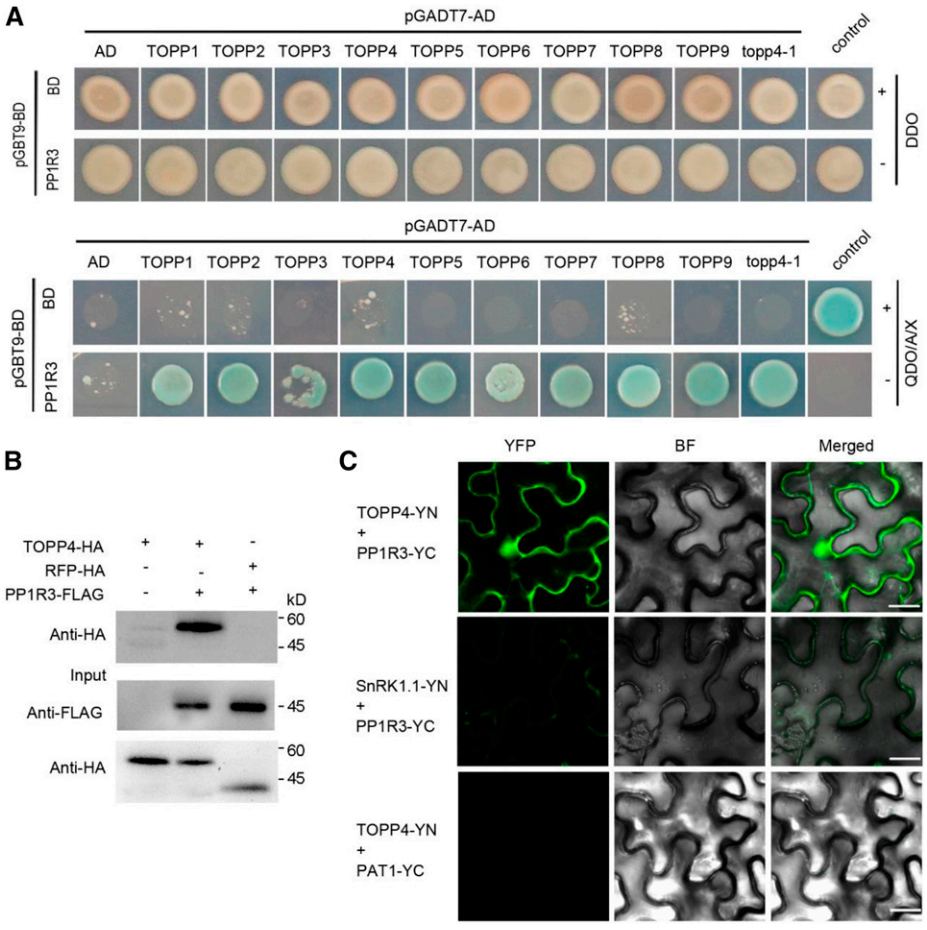

Figure 2. PP1R3 interacts with TOPPs in vitro and in vivo. A, Y2H assay of topp4-1, the topp4 mutant protein encoded by the *topp4-1* allele. DDO, SD/−Leu/−Trp; QDO/A/X, SD/−Leu/−Trp/−His/−Ade supplemented with X-α-Gal and Aureobasidin A; control +/−, positive and negative controls, respectively. B, Co-IP assay. Transient expression of *HA-TOPP4*, *PP1R3-FLAG*, or *RFP-HA* in *Nicotiana benthamiana* epidermal cells for Co-IP. Anti-Flag antibody was used for immunoprecipitation, and anti-HA antibody was used for western blotting. C, BiFC assay. *TOPP4-YN*/*PP1R3-YC*, *TOPP4-YN*/*PAT1-YC*, and *PP1R3-YC*/*SnRK1.1-YN* were coexpressed in *N. benthamiana* epidermal cells. BF, Bright field. Scale bars = 25 μm.

DNA with *GUS* (*proPP1R3:gPP1R3-GUS*/Col). GUS staining indicated that *PP1R3* was widely expressed at various stages of plant development, including imbibed seed, seedling, mature leaves, and floral tissues (Fig. 3C).

PP1R3 Is Involved in ABA and Abiotic Stress Responses

To examine the biological function of *PP1R3*, we examined three independent transfer DNA (T-DNA) insertion mutants of *PP1R3* (Supplemental Fig. S2A). Using reverse transcription quantitative PCR (RT-qPCR), we did not detect full-length *PP1R3* transcripts in *pp1r3-1* and *pp1r3-2* mutants, while the expression of *PP1R3* appeared to be decreased in the *pp1r3-3* mutant (Supplemental Fig. S2B). Compared with Col, the primary roots of *pp1r3-1* and *pp1r3-2* mutants, but not *pp1r3-3* mutants, were slightly shorter, and the rosette leaf diameter of *pp1r3* mutants was smaller (Supplemental Fig. S2, C to E).

Given that PP1R3 interacted with TOPPs, we determined whether PP1R3 was involved in hormone signaling like TOPPs. We found that compared to Col, *pp1r3-1* and *pp1r3-2* mutants were more sensitive to exogenous ABA (Fig. 4). After ABA treatment, *pp1r3* mutants showed reduced seed germination and cotyledon greening, slower seedling growth (Fig. 4, A–C), and shorter primary roots compared with Col (Fig. 4, D and E). The phenotypes of *pp1r3-1* and *pp1r3-2* were rescued by the *PP1R3* genomic DNA under its native promoter (Fig. 4). This confirmed that the ABA-hypersensitive phenotypes of *pp1r3* mutants were due to loss of function of *PP1R3*.

Since ABA is a key phytohormone in stress adaptation, we tested whether *PP1R3* participated in the response to abiotic stresses. Under high-salinity conditions, the germination and cotyledon greening of *pp1r3-1* and *pp1r3-2* were reduced compared to Col, and the *pp1r3* mutants grew more slowly than Col (Fig. 5, A–C). As expected, the defective phenotypes of *pp1r3* mutants were recovered by *PP1R3* (Fig. 5, A–C). In addition, after drought treatment, the recovery of *pp1r3* mutants was better than Col, and the percent survival of *pp1r3* mutants was significantly higher than those of Col and the two complemented lines (Fig. 5D). Furthermore, we found that after Col seedlings were treated with ABA or abiotic stresses (high concentrations of NaCl, mannitol, and Suc), the expression of *PP1R3* was significantly inhibited (Fig. 5E). These results indicated that *PP1R3* is involved in ABA and abiotic stress responses.

PP1R3 Genetically Interacts with *TOPPs*

To further verify the participation of TOPPs in ABA and abiotic stress responses, we obtained several *topp*

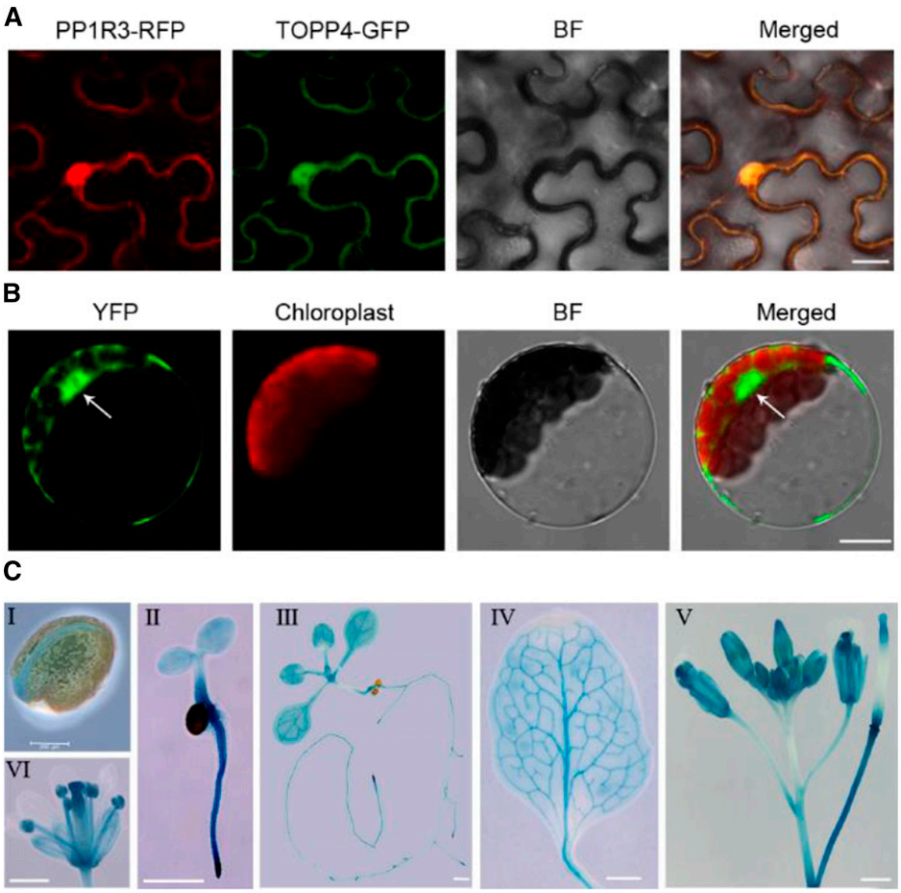

Figure 3. Subcellular localization of PP1R3 and tissue-specific expression of *PP1R3*. A, Subcellular localization of PP1R3 and TOPP4. *PP1R3-RFP* was coexpressed in *N. benthamiana* epidermal cells with *TOPP4-GFP*. BF, bright field. Scale bar = 20 μm. B, Subcellular localization of PP1R3 in Arabidopsis. *PP1R3-YFP* was expressed in the protoplast of Arabidopsis mesophyll cells. Chloroplast, Chloroplast autofluorescence; BF, bright field. The arrow indicates the nucleus. Scale bar = 10 μm. C, Expression patterns of *PP1R3*. The *PP1R3* genomic fusion with a *GUS* reporter driven by the *PP1R3* promoter was used for GUS staining. Shown are an imbibed seed (I), a 3-d-old seedling (II), a 10-d-old seedling (III), a mature leaf (IV), and floral tissues (V and VI). Scale bars = 200 μm (I) and 500 μm (II to VI).

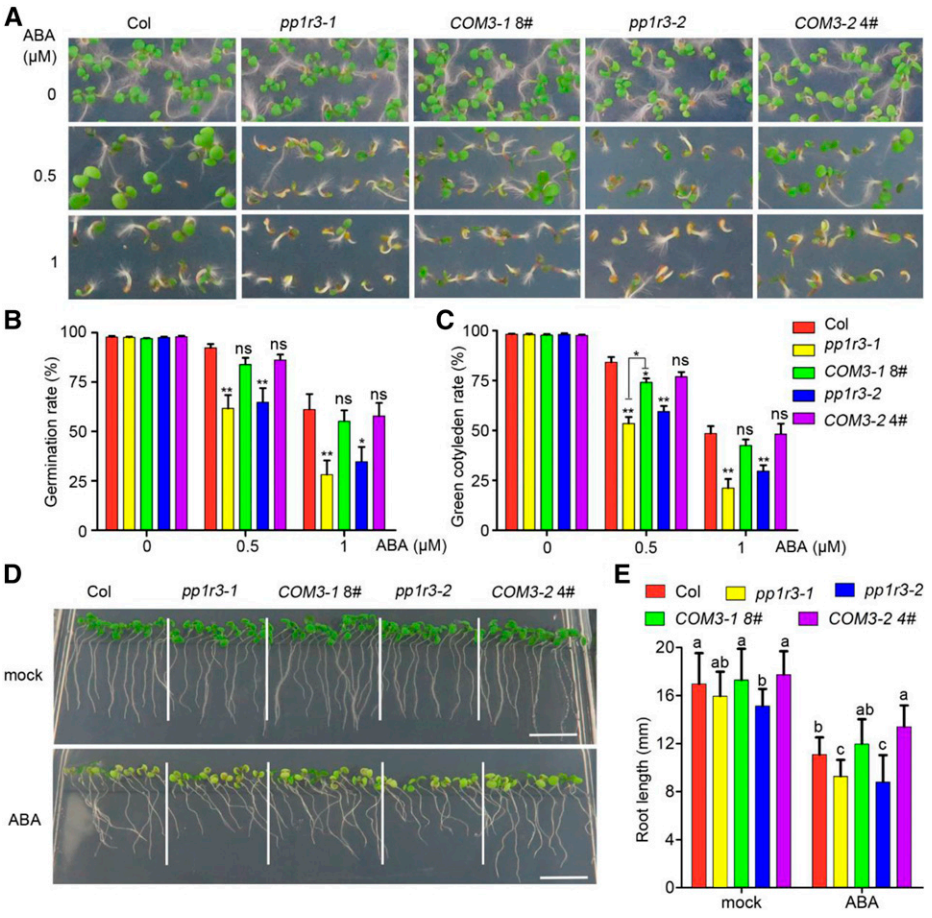

Figure 4. *pp1r3* mutants are more sensitive to ABA. A, Phenotypes of seedlings at 5 DAG on 0.5× MS agar plates with different concentrations of ABA. B and C, Germination rates at 3 DAG (B) and green cotyledon rates at 5 DAG (C) for the seedlings shown in A, expressed as the mean ± SE of $n = 5$ biological replicates. More than 50 seeds were used per line in each experiment. *COM3-1* and *COM3-2* represent the complementary lines *proPP1R3:gPP1R3/pp1r3-1* and *proPP1R3:gPP1R3/pp1r3-2*, respectively. Asterisks indicated statistical significance as determined by Student's *t* test (*$P < 0.05$ and **$P < 0.01$). ns, No significant difference,. In the statistics analysis, except for the comparison between *pp1r3-1* and *COM3-1* line 8, results of significant analyses were compared with Col. D, Phenotypes of primary roots after ABA treatment. Seedlings were grown for 3 d on 0.5× MS agar plates, then transferred to 0.5× MS agar plates with or without 5 μM ABA for 5 d. Scale bars = 1 cm. E, Lengths of primary roots are expressed as the mean ± SD of $n > 30$ roots. The experiment was repeated three times. Lowercase letters indicate statistical significance using one-way ANOVA followed by Fisher's least significant difference test ($P < 0.05$).

loss-of-function mutants by identifying T-DNA insertion mutants and using CRISPR/Cas9 (Supplemental Fig. S3, A and B). The mutants included *topp4-3*, *topp5-cas*, *topp8-cas*, the *topp8-cas topp9* (*topp8 topp9*) double mutant, *topp6/topp7/topp9* triple mutants, *topp1/2/4-3/6/7/9* sextuple mutants (*topp-6m*), and *topp1/4-3/5-cas/6/7/8-cas/9* septuple mutants (*topp-7m*; Liu et al., 2020). As expected, multiple mutants, such as *topp8 topp9*, *topp6/7/9*, *topp-6m*, and *topp-7m*, were hypersensitive to ABA and high salinity, similar to the *pp1r3* mutants (Fig. 6, A and B). For example, under treatment with ABA and NaCl, the percentages of green cotyledons in *topp-7m* were 28% ± 2.4% and 37.5% ± 1.2%, respectively, significantly less than in Col (57.8% ± 3.2% and 55.7% ± 4.7%, respectively; Fig. 6B).

Our results suggested that *PP1R3* and *TOPPs* should also interact genetically. To verify this hypothesis, RNA-sequencing (RNA-Seq) was performed to reveal the genetic relationship between *PP1R3* and *TOPPs* (Supplemental Fig. S4A; Supplemental Table S2). Cluster analysis results showed that a large number of genes had similar expression trends in *pp1r3-2* and *topp-7m* (Fig. 6C; Supplemental Fig. S4A). RNA-Seq revealed that there were 746 differentially expressed genes (DEGs) in *pp1r3-2* versus Col and 545 DEGs in *topp-7m* versus Col (Fig. 6D; Supplemental Fig. S4B). Surprisingly, there were only 97 DEGs in *pp1r3-2* versus *topp-7m*, which was far less than the number of DEGs in *pp1r3-2* or *topp-7m* versus Col (Fig. 6D; Supplemental Fig. S4B). Among these DEGs, 365 were common in *pp1r3-2* and *topp-7m* compared with Col, accounting for 67% of the DEGs in *topp-7m* (Supplemental Fig. S4B). Of the 365 common DEGs, 234 were co-downregulated (down and down) and 130 co-upregulated (up and up), accounting for 99% of these common DEGs (Fig. 6E; Supplemental Fig. S4B). Gene ontology (GO) analysis showed that multiple biological processes related to the response to ABA and abiotic stimulus were significantly enriched in the DEGs common to *pp1r3-2* and *topp-7m* mutants (Fig. 6F). These results indicated that *PP1R3* and *TOPPs* are involved in similar signaling pathways. Furthermore, if PP1R3 and TOPPs form a complex to participate in ABA and abiotic stress responses, the phenotype of *pp1r3 topp* multiple mutants would be similar to the phenotype of single *pp1r3* or *topp* mutants. We proved that this was true, as expected, through the physiological changes of the *pp1r3 topp1 topp4-3* triple mutant response to ABA and high salinity. After ABA or NaCl treatment, the percent germination of *pp1r3-1 topp1 topp4-3* was significantly lower than that of Col, but not significantly different from those of *pp1r3-1* or *topp1 topp4-3* (Fig. 6, G and H).

To further examine the genetic relationship between *PP1R3* and *TOPPs*, we constructed *pp1r3 topp4-1* double mutants by crossing *pp1r3* with the dominant-negative

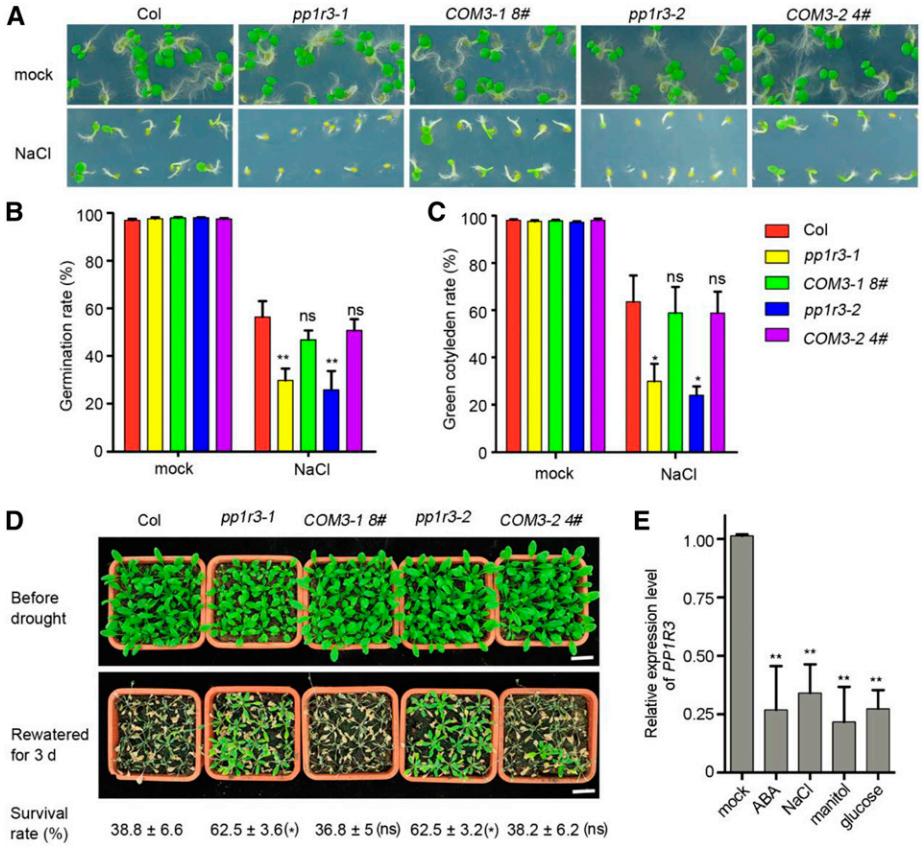

Figure 5. *PP1R3* is involved in abiotic stress responses. A, Phenotypes of seedlings treated with high salinity. Sterile seeds were sown on 0.5× MS agar plates with or without 175 mM NaCl for 5 d after vernalization. B and C, Seed germination rates at 3 DAG (B) and green cotyledon rates at 5 DAG (C) of the seedlings shown in A are expressed as the mean ± SE of $n = 5$ biological replicates, with >50 seeds used per line in each experiment. Asterisks indicated statistical significance as determined by Student's *t* test (*$P < 0.05$ and **$P < 0.01$). ns, No significant difference. D, Drought tolerance experiment. The plants were grown for 10 d under normal conditions, then treated for 10 d with drought, then watered again for 3 d. The experiment was repeated three times, with three pots at a time and 16 seedlings per line in each pot. Scale bars = 2 cm. E, Detection of *PP1R3* expression by RT-qPCR. Ten-day-old Col seedlings were treated with different stresses for 4 h, and the expression of *PP1R3* was detected. *UBQ10* was used as a reference gene. Values are expressed as the mean ± SE of $n = 3$ biological replicates.. Asterisks indicated statistical significance as determined by Student's *t* test (**$P < 0.01$).

mutant *topp4-1* (Supplemental Fig. S3, C and D). Similar to *topp* loss-of-function mutants, *topp4-1* was hypersensitive to ABA, and the phenotype was more severe than that of *pp1r3* (Fig. 7, A and B). Surprisingly, the ABA-sensitive phenotype of *pp1r3 topp4-1* was similar to that of *pp1r3*, indicating that *pp1r3* partially recovered the ABA-hypersensitive phenotype of *topp4-1* (Fig. 7, A and B). Additionally, RNA-Seq revealed that there were 388 common DEGs in *pp1r3-2* versus Col and *pp1r3-2 topp4-1* versus Col, accounting for 52% and 79% of the DEGs of the two mutants, respectively (Supplemental Fig. S4C; Supplemental Table S2). Of the 388 common DEGs, cluster analysis results showed that the relationship between *pp1r3-2* and *pp1r3-2 topp4-1* was very close at the gene level, and the expression patterns of these common DEGs were almost completely identical in *pp1r3-2* and *pp1r3-2 topp4-1* (Fig. 7C; Supplemental Fig. S4C). More importantly, there were only seven DEGs in *pp1r3-2* versus *pp1r3-2 topp4-1*, and under lower screening criteria only 43 DEGs between the two (Fig. 7D; Supplemental Fig. S4D). Notably, in *pp1r3-2 topp4-1* mutants, many genes whose expression level was changed in *topp4-1* could be partially restored to the expression level in *pp1r3-2* (Fig. 7C; Supplemental Fig. S4, A and E). Moreover, *pp1r3* mutants also partially repressed the dwarf phenotype of *topp4-1*, further supporting the genetic interaction between *PP1R3* and *TOPPs* (Fig. 7E). These results support the observation that PP1R3 and TOPPs form a complex and suggest that this complex functions in ABA and abiotic stress responses and other biological processes.

ABA Signaling Is Regulated in Parallel by PP1R3 and ABI1

We identified 148 DEGs associated with ABA and abiotic stress in the *pp1r3-2* and *topp-7m* RNA-Seq data (Supplemental Table S3). Among these, there were 126

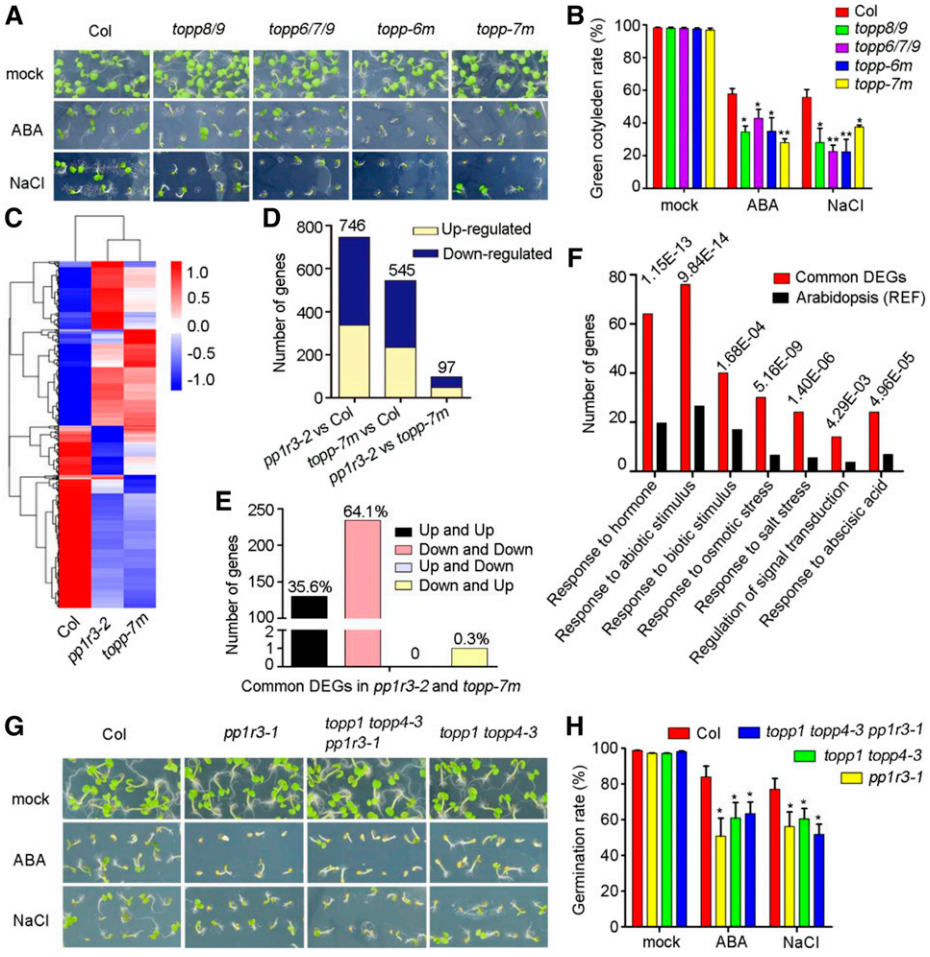

Figure 6. *PP1R3* genetically interacts with *TOPPs*. A, Phenotypes of seedlings treated with ABA or NaCl. Sterile seeds were sown on 0.5× MS agar plates containing 1 μM ABA or 175 mM NaCl and cultured for 5 d after vernalization. B, Green cotyledon rates for *topp8/topp9*, *topp6/7/9*, *topp-6m*, and *topp-7m* mutants. Values are expressed as the mean ± SE of $n = 5$ biological replicates. More than 50 seeds were used per line in each experiment. Asterisks indicated statistical significance as determined by Student's *t* test (*$P < 0.05$ and **$P < 0.01$). C, Heatmap analysis of gene expression trends in *pp1r3-2* and *topp-7m* mutants. The genes analyzed included the overlap of DEGs in *pp1r3-2* and *topp-7m* (as compared with Col). DEGs were defined as |log2 (fold change)| ≥ 1 and adj-$P < 0.05$. Scale value was obtained by zero-mean normalization of the gene expression level (log10 [FPKM+1]) of the sample. D, Analysis of DEGs between *pp1r3-2* and *topp-7m*, showing the expression level of genes increased (Upregulated) or decreased (Downregulated) in the group. Numbers above the bars represent the number of DEGs. E, Analysis of DEGs common to the *pp1r3-2* and *topp-7m* mutants. The genes used included the overlap of DEGs in *pp1r3-2* and *topp-7m*. Up and Up indicates genes upregulated in both mutants, Down and Down genes downregulated in both mutants, Up and Down genes upregulated in *pp1r3-2* and downregulated in *topp-7m*, and Down and Up genes downregulated in *pp1r3-2* and upregulated in *topp-7m*. Percentages above the bars represent the proportion of genes in the group compared to all common DEGs. F, Analysis of biological processes of the DEGs common to *pp1r3-2* and *topp-7m* mutants. Reference (REF) genes were randomly selected from the Arabidopsis database. Some of the biological processes related to abiotic stress and ABA are shown. Numbers displayed in scientific notation indicate the results of statistical analysis after correction for the false discovery rate. G, Phenotypes of *pp1r3-1 topp1 topp4-3* triple mutants after ABA or NaCl treatment. Sterile seeds were sown on 0.5× MS agar plates containing 1 μM ABA or 175 mM NaCl and cultured for 3 d after vernalization. H, Germination rates at 3 DAG, expressed as the mean ± SE of $n = 5$ biological replicates. More than 50 seeds were used per line in each experiment. Asterisks indicated statistical significance as determined by Student's *t* test (*$P < 0.05$).

DEGs in *pp1r3-2*, 98 DEGs in *topp-7m*, and 76 common DEGs. Moreover, the heatmap of these DEGs revealed many genes that showed similar expression trends in *pp1r3-2* and *topp-7m* mutants (Fig. 8A). Subsequently, we used RT-qPCR to detect the expression levels of some important genes involved in ABA or abiotic stress in *pp1r3-2* and *topp-7m*. Compared with Col, expression of the ABA transporter gene *ATP-Binding Cassette G40* (*ABCG40*) and the ABA receptor genes *PYL5* and *PYL6* was increased significantly in the *pp1r3-2* and *topp-7m* mutants (Fig. 8B). By contrast, expression of the transcription factor genes *ABA Responsive Elements-Binding*

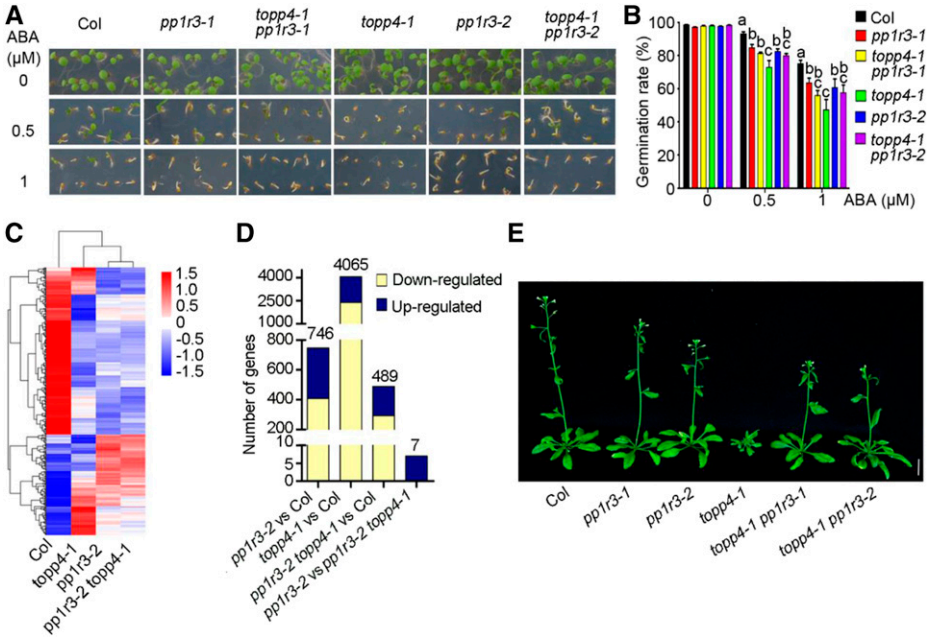

Figure 7. *pp1r3* mutants partially restore the phenotype of *topp4-1*. A, Phenotypes of seedlings treated with different concentrations of ABA. B, Germination rates at 3 DAG expressed as the mean ± SE of $n = 5$ biological replicates. More than 50 seeds were used per line in each experiment. Lowercase letters indicate statistical significance using one-way ANOVA followed by Fisher least significant difference test ($P < 0.05$). C, Heatmap analysis of gene expression trends of the DEGs common to *pp1r3-2*, *topp4-1*, and *pp1r3-2 topp4-1* mutants. Genes used represent the overlap of DEGs in *pp1r3-2*, *topp4-1*, and *pp1r3-2 topp4-1* (compared with Col). Scale value reflected the gene expression level of the sample. D, Analysis of DEGs between *pp1r3-2* and *pp1r3-2 topp4-1*, showing the expression levels of genes in the group that were upregulated or downregulated relative to Col. Numbers above the bars indicate the number of DEGs. E, Phenotypes of 4-week-old plants. Scale bar = 1 cm.

Factor2 (*ABF2*) and *ABA Insensitive5* (*ABI5*), and the stress-induced genes *Responsive to Dehydration29A* (*RD29A*) and *Cold-Regulated15A* (*COR15A*), were decreased significantly in the mutants (Fig. 8B). The ABA biosynthetic enzyme genes *NCED3* and *Abscisic Aldehyde Oxidase3* (*AAO3*), transporter gene *ABCG25*, and signal pathway gene *SnRK2.6* were slightly downregulated in *pp1r3-2* and *topp-7m*, whereas other genes showed no significant changes (Fig. 8B). Together, the results indicated that ABA signaling is changed in the *pp1r3* and *topp-7m* mutants.

ABI1 belongs to the PP2CA family and plays a key role in ABA signaling (Umezawa et al., 2009). We therefore examined whether PP1R3 interacts physically or genetically with ABI1. After ABA treatment, the root lengths of *pp1r3-1 abi1-1c* and *pp1r3-2 abi1-1c* seedlings were significantly longer than those of Col, *pp1r3-1*, and *pp1r3-2* (Fig. 8, C and D). However, the root length of *pp1r3 abi1-1c* seedlings was significantly reduced in an ABA dose-dependent manner compared with *abi1-1c* (Fig. 8, C and D), indicating that *pp1r3 abi1-1c* showed an additive effect of the *pp1r3* and *abi1-1c* mutations in response to ABA. Additionally, no physical interaction between PP1R3 and ABI1/ABI2 was detected using Y2H assays (Supplemental Fig. S5). The results revealed that *PP1R3* and *ABI1* regulate ABA responses in parallel.

PP1R3 Inhibits TOPP Activities

Based on the above results, it was considered that PP1R3 acted as a regulatory subunit of TOPPs to form PP1R3:TOPP holoenzymes, which participate in ABA responses. We verified whether PP1R3 regulated the enzymatic activity of TOPPs by using the compound 4-nitrophenylphosphate (pNPP) as a substrate of PP1 to detect phosphatase activity of TOPPs. Changes in 4-nitrophenol (pNP) content, the hydrolysate of pNPP, and TOPP activities were indicated by altered absorption at 405 nm (ΔA405). We found that pNP increased with increasing TOPP4-His concentration (Fig. 9A). Compared to TOPP4-His alone, when PP1R3-GST was added, pNP increased more slowly (Fig. 9A), indicating that PP1R3 inhibits the hydrolysis of pNPP by TOPP4. As a control, another TOPP4-interaction protein, Mitogen-Activated Protein Kinase6 (MPK6; Table 1; Liu et al., 2020), did not affect the hydrolytic ability of TOPP4 (Fig. 9A). We further examined the inhibition by PP1R3 of other TOPPs. Similar to TOPP4, the ability of TOPP1-His, TOPP3-His, and TOPP9-His to hydrolyze pNPP decreased with increasing PP1R3. Thus, our results indicated that PP1R3 inhibits the catalytic activity of TOPPs in vitro.

PP1R3 Facilitates the Nuclear Localization of TOPP4

To investigate whether PP1R3 affected the subcellular localization of TOPPs, we constructed transgenic

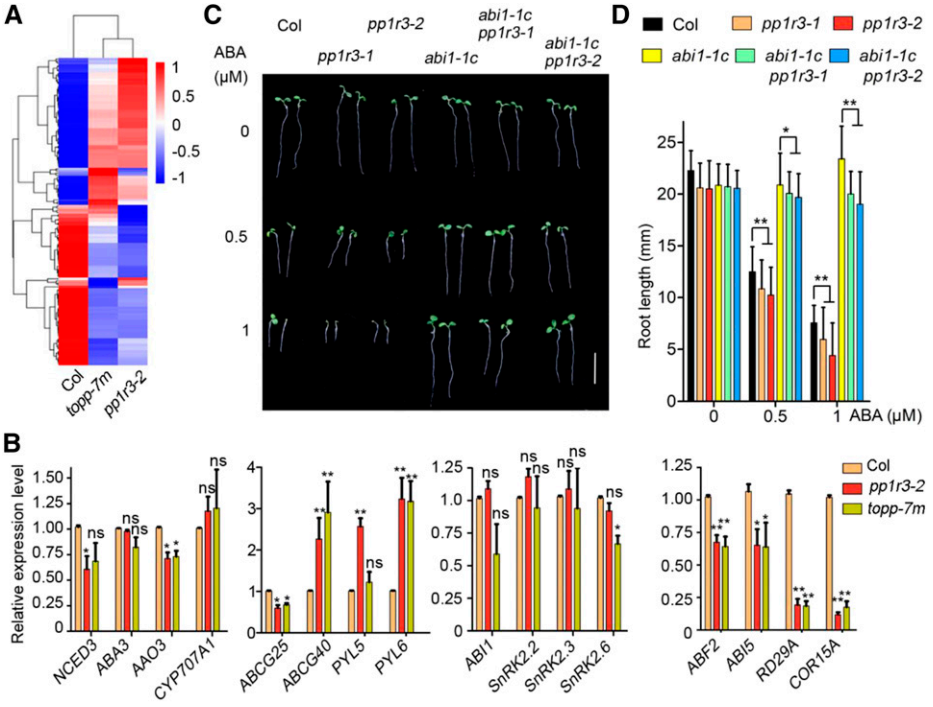

Figure 8. Alteration of the ABA signaling pathway in *pp1r3* mutants. A, Heatmap analysis of gene expression trends of the DEGs associated with ABA and abiotic stress in *pp1r3-2* and *topp-7m*. Scale values reflect gene expression levels of the sample. B, Verification of the expression levels of ABA-related genes in *pp1r3-2* and *topp-7m* measured by RT-qPCR. *UBQ10* was used as a reference gene. Values are expressed as the mean ± SE of $n = 3$ biological replicates. Asterisks indicated statistical significance as determined by Student's *t* test (*$P < 0.05$ and **$P < 0.01$). ns, No significant difference. C and D, Phenotypes of primary roots treated with ABA (C), and the statistical results (D). Sterilized seeds were cultured on ABA-containing plates for 7 d, and root lengths then were measured using ImageJ software. *abi1-1c* is the *abi1-1* mutant in the Col background. Values are expressed as the mean ± SD of $n > 30$ roots. Scale bar = 1 cm. The experiment was repeated three times. Asterisks indicated statistical significance as determined by Student's *t* test (*$P < 0.05$ and **$P < 0.01$).

lines overexpressing *TOPP1-GFP* and *TOPP4-GFP* in Col and *pp1r3* mutants. Because TOPP1-GFP was almost undetectable in the *pp1r3* mutants, we focused on TOPP4-GFP (Supplemental Fig. S6). The fluorescence of TOPP4-GFP was slightly increased in the cytoplasm of *pp1r3-1* and *pp1r3-2* compared with Col (Fig. 10, A and B). The relative nucleus/cytoplasm fluorescence (N/C) ratios were less in *pp1r3-1* and *pp1r3-2* (3.3 ± 1.3 and 4.1 ± 1.3, respectively) than in Col (4.9 ± 1.8; Fig. 10C). We also detected the distribution of TOPP4-GFP in the nucleus and cytoplasm by immunoblotting and found that the N/C ratio of TOPP4-GFP was decreased in *pp1r3* compared to Col (Fig. 10D). These results indicated that PP1R3 promotes TOPP4 localization to the nucleus.

Nuclear Localization of TOPP4 Is Important for ABA Signaling

We further investigated the subcellular localization of TOPPs in response to ABA. After ABA treatment, TOPP1-GFP and TOPP4-GFP signals increased in the cytoplasm but decreased in the nucleus, suggesting that TOPPs were transported from the nucleus to the cytoplasm in response to ABA (Fig. 11A). To test this hypothesis, we constructed TOPP4 with a nuclear export signal (NES-TOPP4) or nuclear localization signal (NLS-TOPP4) and expressed these proteins in transgenic lines in the *topp4-1* background. We found the TOPP4-GFP fusion proteins in the *35S:NES-TOPP4-GFP/topp4-1* and *35S:NLS-TOPP4-GFP/topp4-1* transgenic lines localized in the cytoplasm and nucleus, respectively, as expected (Fig. 11B). Overexpression of *TOPP4* and *NLS-TOPP4* partially restored the ABA-hypersensitive phenotype of *topp4-1*, but overexpression of *NES-TOPP4* could not, suggesting that TOPP4 localization in the nucleus was important for restoring the ABA-hypersensitive phenotype of *topp4-1* (Fig. 11, C and D). These results implied that the nuclear localization of TOPP4 plays a key role in ABA signaling.

DISCUSSION

PP1R3 Is a Regulatory Subunit of TOPPs in Arabidopsis

Arabidopsis has >1,000 protein kinases, but only ~150 protein phosphatases (Kerk et al., 2008; Lehti-Shiu

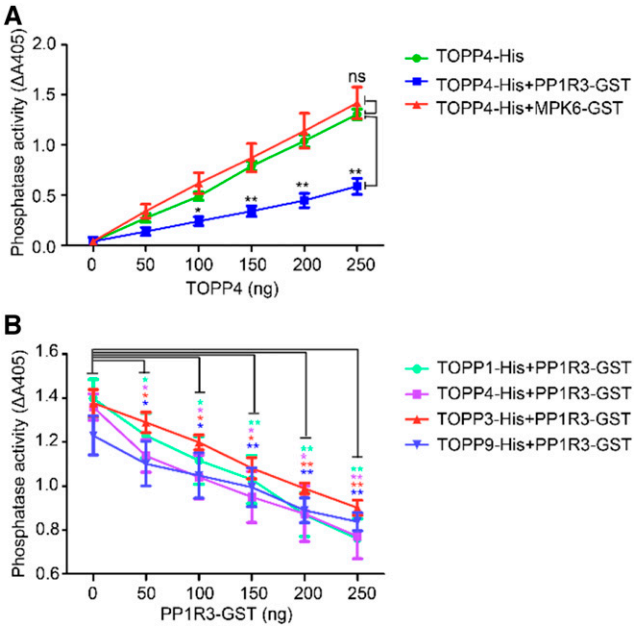

Figure 9. PP1R3 inhibits the phosphatase activity of TOPPs, as shown by phosphatase activity assay. (A) The content of TOPP4 was gradually increased while that of PP1R3-GST and MPK6-GST remained unchanged (250 ng). B, The amount of TOPP-His proteins remained constant (250 ng while the content of PP1R3-GST gradually increased. Changes in TOPP phosphatase activities were indicated by changes in the absorption values at 405 nm (ΔA405). Values are recorded as the mean ± SE, $n = 3$ biological replicates. Significance results are color coded according to the key: Asterisks indicated statistical significance as determined by Student's *t* test (*$P < 0.05$ and **$P < 0.01$). ns, No significant difference.

and Shiu, 2012). Therefore, there could be many phosphatase-specific interacting proteins to ensure the specificity of phosphatases for the correct substrates. Our knowledge about PP1 has increased, but only a few PP1rs are known in plants so far (Takemiya et al., 2009, 2013; Templeton et al., 2011; Boevink et al., 2016). Here, we identified a PP1 regulatory subunit, PP1R3, which regulates the enzyme activity and nuclear localization of TOPPs in Arabidopsis. The C terminus of PP1R3 is important for its interaction with TOPPs, and the interaction between PP1R3 and TOPP4 depends on the N terminus of TOPP4 (Supplemental Fig. S1). These results reveal that the interaction of PP1R3 and TOPPs in Arabidopsis is similar to that of SDS22 and PP1c in humans (Ceulemans et al., 2002). SDS22, the human and yeast (*Saccharomyces cerevisiae*) homolog of PP1R3, not only regulates the nuclear localization and enzymatic activity of PP1c but also interacts with INH3 to promote PP1c biogenesis in budding yeast and human Hela cells (Cheng and Chen, 2015; Weith et al., 2018). Because we observed that the accumulation of TOPP1-GFP protein was drastically decreased in *pp1r3* mutants compared with Col (Supplemental Fig. S6A), we speculate that PP1R3 also regulates TOPP biogenesis or turnover. Additionally, we found that high expression of *PP1R3* by *pGBTK7-PP1R3* and *pGADT7-PP1R3* in yeast could be lethal (Supplemental Fig. S7). This may result from the different physiological functions of PP1R3 and SDS22. The main function of SDS22 is to colocalize with PP1c on kinetochores to regulate chromosome segregation and cell division (Posch et al., 2010; Moreira et al., 2019). PP1R3 binds to PP1c competitively with SDS22 in yeast, interfering with the SDS22-PP1c interaction and leading to abnormal PP1c activity. The absence of SDS22 or abnormal PP1c activity leads to abnormal cell morphology or cell death in yeast (Pinsky et al., 2006; Robinson et al., 2012). Therefore, although PP1R3 is similar to SDS22 in structure and biochemistry, its physiological function is different in plants.

PP1R3 Genetically Interacts with *TOPPs* in ABA and Abiotic Stress Responses

We showed that the *pp1r3* and *topp* mutants were more sensitive to ABA and high salinity, and about two-thirds of DEGs in *topp-7m* showed the same changes as in *pp1r3-2* (Fig. 6). Likewise, the *pp1r3* and *pp1r3-2 topp4-1* mutants showed great similarities in physiology and gene expression (Fig. 7). Furthermore, the responses of *pp1r3-1 topp1 topp4-3* and *pp1r3 topp4-1* to ABA were consistent with those of *pp1r3-1*. These results indicate that *PP1R3* and *TOPPs* perform similar functions interdependently and indispensably. It appears that our genetic evidence is inconsistent with the biochemical results that PP1R3 inhibits TOPP phosphatase activities (Fig. 9). In fact, PP1r can promote the function of the PP1 holoenzyme in vivo, including increasing the concentration of PP1c in specific cell compartments, promoting the assembly of the holoenzyme, and improving the ability of the holoenzyme to recruit substrates (Heroes et al., 2013; Verbinnen et al., 2017). Most PP1rs are known to inhibit the phosphatase activity of PP1c in vitro, but it is commonplace that the phenotype of the *pp1r* mutant is similar to that of the *pp1c* mutant. For instance, knocking out the PP1 inhibitor *Nuclear Inhibitor of PP1* (*NIPP1*) leads to hyperphosphorylation of the PP1 substrate Enhancer of Zeste Homolog2 (EZH2) and is consistent with the phenotype of knocking out *PP1c* in mice (*Mus musculus*; Ferreira et al., 2018).

We found that *topp4-1* was more sensitive to ABA than *pp1r3* (Fig. 7, A and B), whereas *topp1 topp4-3* and *pp1r3-1* were similarly sensitive (Fig. 6, G and H). This indicated that the mutant topp4-1 protein interfered with TOPP protein function in the ABA response in a dominant-negative manner, resulting in increased ABA sensitivity of *topp4-1* compared to *topp1 topp4-3* double mutants. This phenomenon is consistent with our previous report that the phenotypes of *topp4-1* are more severe than those of *topp-7m* in plant morphology and gene expression (Supplemental Fig. S4; Liu et al., 2020). More importantly, in *pp1r3 topp4-1* double mutants, *pp1r3* mutants can partially rescue the

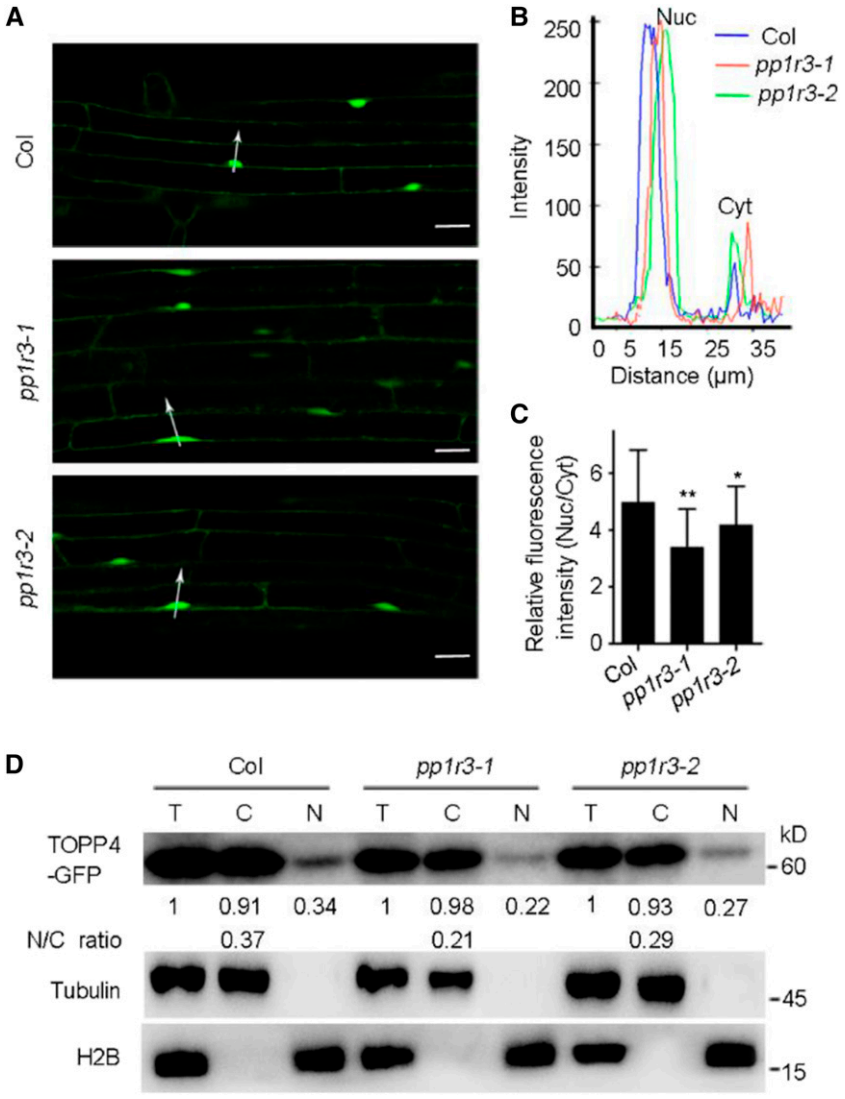

Figure 10. PP1R3 facilitates nuclear localization of TOPP4. A, Localization of TOPP4-GFP in root cells of Col and *pp1r3* mutants. Scale bars = 20 μm. B and C, Fluorescence intensity curves (B) and relative N/C ratios (C). Fluorescence intensity was determined in the direction along the arrow drawn on the confocal image using LAS AF Lite software. Values are expressed as the mean ± SD of $n > 100$ cells. Asterisks indicated statistical significance as determined by Student's t test ($^*P < 0.05$ and $^{**}P < 0.01$). The experiment was repeated three times. D, Detection of TOPP4-GFP localization by nuclear-cytoplasmic fractionation. The numbers under the lanes indicate the relative protein content, with the value of total protein in each line set to 1 using ImageJ software. T, C, and N represent total, cytoplasmic, and nuclear protein, respectively. α-tubulin and histone H2B were used as cytoplasmic and nuclear markers, respectively. The experiment was repeated three times.

topp4-1 ABA-hypersensitive phenotype (Fig. 7, A and B). Therefore, we supposed that the dominant negative function of topp4-1 protein in response to ABA is also dependent on its interaction with PP1R3. So, when *PP1R3* is absent, the ABA-hypersensitive phenotype of *pp1r3 topp4-1* is more similar to that of *pp1r3* than that of *topp4-1*. By the same token, in terms of gene expression and plant morphogenesis, *pp1r3* mutants can partially restore the corresponding phenotypes of *topp4-1* (Fig. 7). Moreover, we have recently reported that the *topp4-1* mutant is an autoimmune activated mutant with high expression of many immune-related genes (Yan et al., 2019; Liu et al., 2020). In *pp1r3-2 topp4-1*, the large number of highly expressed DEGs related to plant immunity in *topp4-1* was partially restored by *pp1r3-2* (Supplemental Fig. S4E). This may be another reason why *pp1r3* mutants partially restore the dwarf phenotype of *topp4-1*. Overall, PP1R3 acts with TOPPs in response to ABA and many other biological processes.

The PP1R3:TOPPs Holoenzyme May Function in Parallel with ABI1 in the Nucleus to Regulate ABA Signaling

The nuclear location of TOPP4 is important for restoring the ABA-hypersensitive phenotype of *topp4-1*, indicating that TOPP4 competes with the topp4-1 mutant protein in the nucleus for ABA response (Fig. 11). We also found that TOPPs can be transported from the nucleus to the cytoplasm under ABA treatment (Fig. 11). Recently, it was reported that Enhancer of ABA Co-Receptor1 (EAR1) regulates ABA signaling by promoting PP2CA enzyme activity, and ABA treatment causes EAR1 to accumulate in the nucleus (Wang et al., 2018). Therefore, we concluded that the nuclear localization and phosphatase activities of TOPPs are important for TOPPs-mediated ABA signaling, which is regulated by PP1R3 during the ABA response. Our result indicated that the root growth of *pp1r3 abi1-1c* in response to ABA showed an additive effect of the two mutants *pp1r3* and *abi1-1c*, but not an epistatic effect of

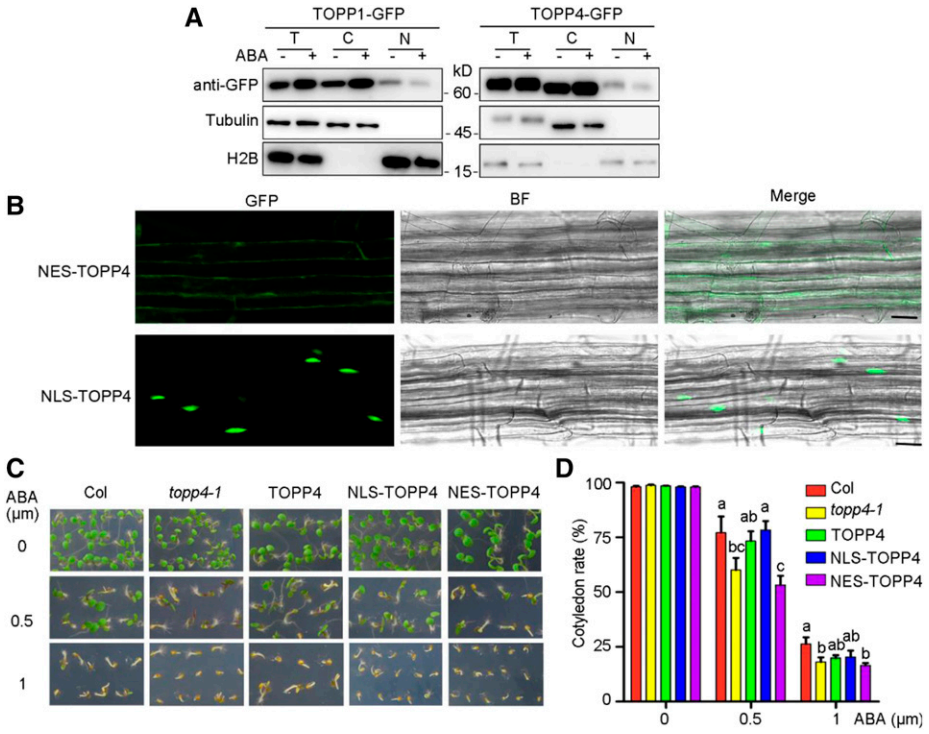

Figure 11. TOPP4 localization in the nucleus plays a key role in TOPPs-mediated ABA signaling. A, Detection of localization changes of TOPP1 and TOPP4 after ABA treatment. Ten-day-old seedlings were treated (+) or not treated (−) with 50 μM ABA for 4 h. T, C, and N represent total, cytoplasmic, and nuclear protein, respectively. TOPP1-GFP and TOPP4-GFP were detected by anti-GFP antibody. α-tubulin and histone H2B were used as cytoplasmic and nuclear markers, respectively. The experiment was repeated three times. B, Subcellular localization of NES-TOPP4 and NLS-TOPP4 in transgenic line root cells. Scale bars = 20 μm. BF, Bright field. C, Phenotypes of seedlings treated with ABA. D, Seedling cotyledon rates at 5 DAG. TOPP4, *35S:TOPP4-GFP/topp4-1*; NES-TOPP4, *35S:NES-TOPP4-GFP/topp4-1*; NLS-TOPP4, *35S:NLS-TOPP4-GFP/topp4-1*. Values are expressed as the mean ± SE of $n = 3$ biological replicates. More than 50 seeds were used per line in each experiment. Lowercase letters indicate statistical significance using one-way ANOVA followed by Fisher's least significant difference test ($P < 0.05$).

abi1-1c (Fig. 8). This genetic relationship is analogous to that of transcription factors MYB30 and ABI5, which regulate parallel pathways during germination in response to ABA (Zheng et al., 2012). In addition, PP1R3 interacted with TOPPs specifically, but did not interact with ABI1 and ABI2 (Supplemental Fig. S5). Many studies report that transcription factors downstream of ABA can regulate ABA synthesis and signal transduction through a regulatory feedback loop (Zong et al., 2016; Tan et al., 2018; Wang et al., 2019). For example, ABFs activated by ABA promote the expression of the ABA coreceptor genes *ABI1* and *ABI2*, which in turn inhibit ABA signaling through dephosphorylation of ABFs (Wang et al., 2019). Hence, we speculate that the PP1R3:TOPPs holoenzyme regulates the response of ABA and the expression of ABA-related genes in parallel with ABI1 by dephosphorylating some transcription factors in the nucleus.

CONCLUSION

We identified a TOPP-interacting protein, PP1R3, in Arabidopsis by mass spectrometric analysis. PP1R3 inhibits the activity of TOPPs and promotes their nuclear localization. As a regulatory subunit of TOPPs, PP1R3 participates in TOPP-mediated pathways, including the response to ABA and abiotic stress. Moreover, the PP1R3:TOPPs holoenzyme may function in parallel with ABI1 in the nucleus to regulate ABA signaling. The identification of PP1R3 provides a new way to study the role of PP1-mediated protein phosphorylation in plant stress responses.

MATERIALS AND METHODS

Plant Materials

Arabidopsis (*Arabidopsis thaliana*) and *Nicotiana benthamiana* plants were grown in a greenhouse under a 16-h light/8-h dark photoperiod at 23°C. Sterilized seedlings were grown on one-half strength Murashige and Skoog medium with 1% (w/v) agarose (0.5× MS agar plates). Arabidopsis ecotype Columbia (Col) was used in this study. *abi1-1c*, the *abi1-1* mutant in the Col background. The T-DNA insertion mutants were *topp4-3* (SALK_098324), *pp1r3-1* (SALK_069235), *pp1r3-2* (SALK_151989), *pp1r3-3* (SALK_054653), *topp1* (SALK_057537), *topp2* (GK-187C10-014623/CS305848), *topp7* (SALK_023073), *topp6* (SALK_093747), and *topp9* (SALK_045433C). Moreover, the mutant *topp-7m* was constructed by knocking out *topp8* and *topp5* in the mutant *topp1/topp4-3/topp6/topp7/topp9* by the CRISPR/Cas9 system. In this paper, the mutants

edited by the CRISPR/Cas9 system were Cas9-free. The CRISPR/Cas9 vector (*pHEE401-2gR*) was isolated using a hygromycin resistance screening system. The validation of *topps* T-DNA mutants and the method for constructing *topps* mutants by the CRISPR/Cas9 system were reported in detail in our previous paper (Liu et al., 2020).

Mass Spectrometric Analysis

The process of affinity purification of GFP fusion protein by anti-GFP antibody was based on a previously published article (Yan et al., 2019). Three-week-old GFP or TOPP4-GFP transgenic plants were used. The purified GFP and TOPP4-GFP fusion proteins and their coprecipitated proteins were isolated by using SDS-PAGE and staining with Coomassie blue. The gels were cut into multiple individual bands based on the brightness and sharpness of the strips, i.e. narrower strong staining bands and wider low staining bands. The cut gel bands were washed with 30% (v/v) acetonitrile containing 100 mM NH_4HCO_3 until these bands were colorless, then dried under vacuum. Next, the bands were analyzed by in-gel digestion followed by liquid chromatography-electrospray tandem mass spectrometry (Orbitrap Fusion Lumos Easy 1200 Nano LC, Thermofisher). The steps after gel decolorization were performed according to methods described in the literature (Wang et al., 2013).

Protein Sequence Analysis

For protein homology analysis, candidate proteins with high sequence identity with PP1R3 protein were searched using the National Center for Biotechnology Information database. The phylogenetic tree was constructed using Geneious R6 by the neighbor-joining method, using the Jukers-Cantor genetic distance model. Interior branch tests were conducted to assess statistical significance of the phylogenetic trees using 1,000 replicates. The scale bar represents the amino acid substitutions per site for a unit branch length (Supplemental Fig. S1A).

Plasmid Construction and Plant Transformation

To construct transgenic plants with GFP tags, the coding sequence (CDS) of *TOPP1* or *TOPP4* was linked to the *pCAMBIA1300-GFP* vector. To construct NES-TOPP4 and NLS-TOPP4, two signal peptide sequences, ATGAACGAG CTTGCTCTTAAG-TTGGCTGGACTTGATATTAACAAGACTGGAGGA (encoding peptide, MNELALKLAGLDINKTGG) and ATGCCTAAGAAGAAG AGAA-AGGTTGGAGGAGGA (encoding peptide, MPKKKRKVGGG) were integrated upstream of the CDS of *TOPP4*. For the construction of GUS staining lines and *PP1R3* complementary lines, the genomic sequences of *PP1R3* (excluding and including the terminator, respectively) driven by the *PP1R3* native promotor (~1.8 kb) were inserted into the *pCAMBIA1305.2-GUS* vector. The CDSs of *TOPP4*, *SnRK1.1*, *RFP*, *PP1R3*, and *PAT1* (*AT1G79090*) were cloned into *pEearleygate202-YC* or *pEearleygate201-YN* BiFC vectors through the Gateway system for BiFC analysis and Co-IP. To generate the Arabidopsis transgenic lines, plants were transformed with *Agrobacterium tumefaciens* strain GV3101 carrying different constructs by a standard genetic floral dipping method (Clough and Bent, 1998).

Y2H Analysis

For Y2H analysis, a bait protein is expressed as a fusion to the Gal4 DNA-binding domain (BD), while libraries of prey proteins are expressed as fusions to the Gal4 activation domain (AD; Clontech, www.clontech.com). The bait plasmid *pGBT9-BD* was used to build *PP1R3-BD* or *PP1R3ΔC-BD*, and the prey plasmid was built with *pGADT7-AD*. The low-expression vector *pGBT9-PP1R3-BD* could be used for Y2H analysis. *pGBKT7-53* and *pGBKT7-Lam* were used as positive and negative control bait plasmids, respectively. *pGADT7-T* was used as a control prey plasmid. The transformed yeast was spread onto double-dropout agar plates (synthetically defined medium including every essential amino acid except for Leu and Trp [SD/−Leu/−Trp]; Clontech, www.clontech.com) and cultured for 4 d. Then, a monoclonal colony was transferred to a quadruple-dropout agar plate with X-α-Gal and Aureobasidin A added (SD/−Leu/−Trp/−His/−Adenine/+X-α-Gal/+Aureobasidin A; Clontech, www.clontech.com) and cultured for 3 to 7 d. Subsequently, the growth status and color of yeast colonies was observed.

Histochemical Detection of GUS Activity and Subcellular Localization

GUS staining has been described previously (Qin et al., 2014). The tissues of *proPP1R3:gPP1R3-GUS*/Col transgenic plants were dipped into GUS working solution for 6 to 12 h and then decolorized with 70% (v/v) ethanol. After decolorization, the stained tissues were observed and imaged using a M205A stereomicroscope (Leica).

To identify localization of PP1R3, the CDS of *PP1R3* was cloned into the *pUBC-RFP-Dest* vector through the Gateway system and injected into *N. benthamiana* leaf epidermal cells. The process for transient expression in *N. benthamiana* leaf epidermal cells used in the localization analysis, as well as BiFC and Co-IP experiments, have been described previously (Qin et al., 2014). In addition, the CDS of *PP1R3* was cloned into the *PA7-YFP* vector for transient expression of *PP1R3-YFP* in Arabidopsis mesophyll protoplasts using previously described procedures (Yoo et al., 2007). Confocal laser microscopy (Olympus Fluoview FV1000MPE or Leica TCS SP8) was used to observe fluorescence.

Physiological Experiments Related to Hormone and Abiotic Stress

To measure germination and the green cotyledon rates, sterilized seeds were planted on 0.5× MS agar plates with different treatments, vernalized for 4 d, and then cultured for 3 to 7 d. The germination rate, cotyledon rate, and cotyledon greening rate were calculated at 3, 5, and 7 d after germination (DAG), respectively. For ABA inhibition of primary root growth, sterile seeds were grown on normal 0.5× MS agar plates. At 3 DAG, the seedlings were transferred to 0.5× MS agar plates with or without ABA and then vertically cultured for 4 to 7 d. Root length was measured using ImageJ. For the drought tolerance experiment, plants were grown for 10 d under normal conditions, then treated for 10 d with drought, then watered for 3 d. Three pots were used at a time with 48 seedlings per line, and the experiment was repeated three times.

RT-qPCR Assay

The total RNA extraction and the cDNA synthesis were performed as previously described (Wang et al., 2014). For detection of gene expression changes after ABA or stress treatment, 10-d-old Col seedlings were transferred to 0.5× MS liquid medium under different treatments for 4 h. All RT-qPCR measurements were performed using ABI StepOnePlus Real-Time PCR Systems (Thermo Fisher Scientific) with SYBRPremix Ex Taq (Takara Bio). The housekeeping gene *Ubiquitin 10* (*UBQ10*) was used as a control. Primer sequences for RT-qPCR used in this study are listed in Supplemental Table S4.

RNA-Sequencing Analysis

For RNA-Seq analysis, 3-week-old leaves were used, and three biological replications were performed. Total RNA extraction, library construction, Illumina sequencing, and screening of DEGs were performed by Novogene (https://www.novogene.com/). Differential expression analysis of two conditions/groups (three biological replicates per condition) was performed using the DESeq2 R package (1.16.1) provided by Novogene. DESeq2 provided statistical routines for determining differential expression in digital gene expression data using a model based on the negative binomial distribution. The resulting *P*-values were adjusted using Benjamini and Hochberg (1995)'s approach for controlling the false discovery rate (adjusted *P* value [adj-*P*]). Genes were considered to be differentially expressed when the absolute value of the log2-fold change ratio was ≥1 ($|\log2\ [\text{fold change}]| \geq 1$) and adj-$P < 0.05$ using the DESeq2 R package (Anders et al., 2012; Love et al., 2014). For clustering, we clustered different samples to see the correlation using the hierarchical clustering distance method with the heatmap function. The clustering software package pheatmap in R provided by Novogene was used for clustering, and the data targeted were the DEGs that overlapped. Clustering was performed based on the relative expression level of the gene log2 (ratios). For GO analysis, the screened DEGs were analyzed by the GO analysis Web site Gene Ontology Resource (http://geneontology.org/), supported by the National Human Genome Research Institute. The RNA-Seq data in this study were deposited in the Gene Expression Omnibus (http://www.ncbi.nlm.nih.gov/geo/) under accession number GSE152030.

Expression and Purification of Protein

For the expression of recombinant protein in prokaryotic cells, the CDSs of *PP1R3*, *TOPPs*, and *MPK6* were cloned into the *pET28a* (His tag) or *pGEX-4T-3* (GST tag) vector. *Escherichia coli* strain *Rossetta* was used for expressing recombinant proteins. The induced expression and purification of recombinant proteins was partially optimized based on methods described previously (Templeton et al., 2011). The concentrations of purified proteins were determined by Bradford assay.

For the Co-IP assay, a previously used experimental procedure was followed (Qin et al., 2014). *Flag-PP1R3-YC*, *HA-RFP-YN*, and *HA-TOPP4-YN* were transiently expressed in *N. benthamiana* leaves in different combinations, then the protein was purified for Co-IP after infecting for 3 to 5 d. Anti-Flag or anti-HA beads were used to purify the fusion proteins with the corresponding tags.

Phosphatase Activity Assay

The experimental procedure was consistent with one previously described (Templeton et al., 2011). Two schemes were followed for detection of phosphatase activity. In one scheme, the content of TOPP4 gradually increased (0–250 ng), but the content of PP1R3-GST or MPK6-GST remained unchanged (250 ng). In the other scheme, the amount of TOPP-His proteins was constant (250 ng), and the content of PP1R3-GST gradually increased (0–250 ng). pNP, the hydrolysate of pNPP by TOPPs, had a specific absorption peak at 405 nm (A405). The concentration of pNP and the activities of TOPPs were indicated by the change of A405 absorbance (ΔA405). Significance analysis of phosphatase activities of TOPP after different treatments was conducted based on the same TOPP content.

Nuclear-Cytoplasmic Fractionation

The experimental procedure for nuclear-cytoplasmic fractionation was performed according to a previously described method (Wang et al., 2011). To observe TOPP4 localization changes in *pp1r3* mutants, 10-d-old TOPP4-GFP transgenic seedlings were used. To observe the response of TOPP-GFP subcellular localization to ABA, 10-d-old *35S:TOPP1-GFP*/Col and *35S:TOPP4-GFP*/Col seedlings were treated, or not, with 50 μM ABA for 4 h. α-tubulin was used as a cytoplasmic marker. Histone H2B was used as a nuclear marker. The total proteins and cytoplasmic proteins were normalized with tubulin, and the extracted nuclear proteins were normalized with H2B.

Statistical Analysis

All physiological and biochemical experiments, transcriptome analysis, and RT-qPCR were performed with at least three biological replications. OriginPro 8 (OriginLab, https://www.originlab.com/) was used for significance analysis. For statistical analysis, except for those specifically marked, all statistical values were compared with the value of Col.

Accession Numbers

Arabidopsis Genome Initiative (https://www.arabidopsis.org/) locus identifiers for the genes mentioned in this article are as follows: *PP1R3* (AT5G19680), *TOPP1* (AT2G29400), *TOPP2* (AT5G59160), *TOPP3* (AT1G64040), *TOPP4* (AT2G39840), *TOPP5* (AT3G46820), *TOPP6* (AT5G43380), *TOPP7* (AT4G11240), *TOPP8* (AT5G27840), *TOPP9* (AT3G05580), and *ABI1* (AT4G26080).

SUPPLEMENTAL DATA

The following supplemental materials are available.

Supplemental Figure S1. Identification of the interaction domains between TOPPs and PP1R3.

Supplemental Figure S2. Identification of *pp1r3* T-DNA insertion mutants.

Supplemental Figure S3. Genotyping of *topps* mutants.

Supplemental Figure S4. RNA-Seq analysis of the genetic relationship between *PP1R3* and *TOPPs*.

Supplemental Figure S5. Identification of the interaction between ABI1 and ABI2 and PP1R3.

Supplemental Figure S6. Identification of transgenic plants overexpressing *TOPP1-GFP* or *TOPP4-GFP*.

Supplemental Figure S7. Overexpression of *PP1R3* leads to death in yeast.

Supplemental Table S1. Identifying the coprecipitates of TOPP4-GFP by mass spectrometry.

Supplemental Table S2. Annotation of DEGs in the RNA-Seq analysis.

Supplemental Table S3. DEGs associated with ABA and abiotic stress in *pp1r3-2* and *topp-7m*.

Supplemental Table S4. Primer sequences for RT-qPCR used in this article.

ACKNOWLEDGMENTS

We thank Xinyu Wang for providing Y2H related vectors, ShuhuaYang for *abi1-1C*, Quansheng Qiu for the *pUBC-RFP-Dest* vector, Yong Ding for *topp4-3* seeds, Qijun Chen for the *pHEE401-2gR* vector, and the Core Facility of the School of Life Sciences, Lanzhou University.

Received August 3, 2020; accepted September 9, 2020; published September 18, 2020.

LITERATURE CITED

Anders S, Reyes A, Huber W (2012) Detecting differential usage of exons from RNA-seq data. Genome Res **22:** 2008–2017

Benjamini Y, Hochberg Y (1995) Controlling the false discovery rate: A practical and powerful approach to multiple testing. J R Stat Soc Series B Stat Methodol **57:** 289–300

Boevink PC, Wang X, McLellan H, He Q, Naqvi S, Armstrong MR, Zhang W, Hein I, Gilroy EM, Tian Z, et al (2016) A *Phytophthora infestans* RXLR effector targets plant PP1c isoforms that promote late blight disease. Nat Commun **7:** 10311

Bollen M, Peti W, Ragusa MJ, Beullens M (2010) The extended PP1 toolkit: Designed to create specificity. Trends Biochem Sci **35:** 450–458

Brugière N, Zhang W, Xu Q, Scolaro EJ, Lu C, Kahsay RY, Kise R, Trecker L, Williams RW, Hakimi S, et al (2017) Overexpression of RING domain E3 ligase ZmXerico1 confers drought tolerance through regulation of ABA homeostasis. Plant Physiol **175:** 1350–1369

Ceulemans H, Bollen M (2004) Functional diversity of protein phosphatase-1, a cellular economizer and reset button. Physiol Rev **84:** 1–39

Ceulemans H, Vulsteke V, De Maeyer M, Tatchell K, Stalmans W, Bollen M (2002) Binding of the concave surface of the Sds22 superhelix to the $\alpha4/\alpha5/\alpha6$-triangle of protein phosphatase-1. J Biol Chem **277:** 47331–47337

Cheng YL, Chen RH (2015) Assembly and quality control of the protein phosphatase 1 holoenzyme involves the Cdc48-Shp1 chaperone. J Cell Sci **128:** 1180–1192

Choy MS, Bolik-Coulon N, Archuleta TL, Peti W, Page R (2018) The structure of SDS22 provides insights into the mechanism of heterodimer formation with PP1. Acta Crystallogr F Struct Biol Commun **74:** 817–824

Clough SJ, Bent AF (1998) Floral dip: A simplified method for *Agrobacterium*-mediated transformation of *Arabidopsis thaliana*. Plant J **16:** 735–743

Eiteneuer A, Seiler J, Weith M, Beullens M, Lesage B, Krenn V, Musacchio A, Bollen M, Meyer H (2014) Inhibitor-3 ensures bipolar mitotic spindle attachment by limiting association of SDS22 with kinetochore-bound protein phosphatase-1. EMBO J **33:** 2704–2720

Fang Y, Sathyanarayanan S, Sehgal A (2007) Post-translational regulation of the *Drosophila* circadian clock requires protein phosphatase 1 (PP1). Genes Dev **21:** 1506–1518

Ferreira M, Verbinnen I, Fardilha M, Van Eynde A, Bollen M (2018) The deletion of the protein phosphatase 1 regulator NIPP1 in testis causes hyperphosphorylation and degradation of the histone methyltransferase EZH2. J Biol Chem **293:** 18031–18039

Finkelstein R (2013) Abscisic acid synthesis and response. Arabidopsis Book **11:** e0166

Franck CM, Westermann J, Bürssner S, Lentz R, Lituiev DS, Boisson-Dernier A (2018) The protein phosphatases ATUNIS1 and ATUNIS2 regulate cell wall integrity in tip-growing cells. Plant Cell **30:** 1906–1923

Guo X, Qin Q, Yan J, Niu Y, Huang B, Guan L, Li Y, Ren D, Li J, Hou S (2015) TYPE-ONE PROTEIN PHOSPHATASE4 regulates pavement cell interdigitation by modulating PIN-FORMED1 polarity and trafficking in Arabidopsis. Plant Physiol **167:** 1058–1075

Hauser F, Li Z, Waadt R, Schroeder JI (2017) SnapShot: Abscisic acid signaling. Cell **171:** 1708

Heroes E, Lesage B, Görnemann J, Beullens M, Van Meervelt L, Bollen M (2013) The PP1 binding code: A molecular-lego strategy that governs specificity. FEBS J **280:** 584–595

Hou YJ, Zhu Y, Wang P, Zhao Y, Xie S, Batelli G, Wang B, Duan CG, Wang X, Xing L, et al (2016) Type one Protein Phosphatase 1 and its regulatory protein Inhibitor 2 negatively regulate ABA signaling. PLoS Genet **12:** e1005835

Humphrey SJ, James DE, Mann M (2015) Protein phosphorylation: A major switch mechanism for metabolic regulation. Trends Endocrinol Metab **26:** 676–687

Kamimura D, Katsunuma K, Arima Y, Atsumi T, Jiang JJ, Bando H, Meng J, Sabharwal L, Stofkova A, Nishikawa N, et al (2015) KDEL receptor 1 regulates T-cell homeostasis via PP1 that is a key phosphatase for ISR. Nat Commun **6:** 7474

Kerk D, Templeton G, Moorhead GB (2008) Evolutionary radiation pattern of novel protein phosphatases revealed by analysis of protein data from the completely sequenced genomes of humans, green algae, and higher plants. Plant Physiol **146:** 351–367

Lehti-Shiu MD, Shiu SH (2012) Diversity, classification and function of the plant protein kinase superfamily. Philos Trans R Soc Lond B Biol Sci **367:** 2619–2639

Liu Y, Yan J, Qin Q, Zhang J, Chen Y, Zhao L, He K, Hou S (2020) Type one protein phosphatases (TOPPs) contribute to the plant defense response in *Arabidopsis*. J Integr Plant Biol **62:** 360–377

Love MI, Huber W, Anders S (2014) Moderated estimation of fold change and dispersion for RNA-seq data with DESeq2. Genome Biol **15:** 550

Moreira S, Osswald M, Ventura G, Gonçalves M, Sunkel CE, Morais-de-Sá E (2019) PP1-mediated dephosphorylation of Lgl controls apical-basal polarity. Cell Rep **26:** 293–301

Ohkura H, Yanagida M (1991) *S. pombe* gene *sds22+* essential for a mid-mitotic transition encodes a leucine-rich repeat protein that positively modulates protein phosphatase-1. Cell **64:** 149–157

Pedelini L, Marquina M, Ariño J, Casamayor A, Sanz L, Bollen M, Sanz P, Garcia-Gimeno MA (2007) YPI1 and SDS22 proteins regulate the nuclear localization and function of yeast type 1 phosphatase Glc7. J Biol Chem **282:** 3282–3292

Pinsky BA, Kotwaliwale CV, Tatsutani SY, Breed CA, Biggins S (2006) Glc7/protein phosphatase 1 regulatory subunits can oppose the Ipl1/aurora protein kinase by redistributing Glc7. Mol Cell Biol **26:** 2648–2660

Posch M, Khoudoli GA, Swift S, King EM, Deluca JG, Swedlow JR (2010) Sds22 regulates aurora B activity and microtubule-kinetochore interactions at mitosis. J Cell Biol **191:** 61–74

Qin Q, Wang W, Guo X, Yue J, Huang Y, Xu X, Li J, Hou S (2014) Arabidopsis DELLA protein degradation is controlled by a type-one protein phosphatase, TOPP4. PLoS Genet **10:** e1004464

Robinson LC, Phillips J, Brou L, Boswell EP, Tatchell K (2012) Suppressors of *ipl1-2* in components of a Glc7 phosphatase complex, Cdc48 AAA ATPase, TORC1, and the kinetochore. G3 (Bethesda) **2:** 1687–1701

Shi Y (2009) Serine/threonine phosphatases: Mechanism through structure. Cell **139:** 468–484

Takemiya A, Ariyoshi C, Shimazaki K (2009) Identification and functional characterization of inhibitor-3, a regulatory subunit of Protein phosphatase 1 in plants. Plant Physiol **150:** 144–156

Takemiya A, Yamauchi S, Yano T, Ariyoshi C, Shimazaki K (2013) Identification of a regulatory subunit of protein phosphatase 1 which mediates blue light signaling for stomatal opening. Plant Cell Physiol **54:** 24–35

Tan W, Zhang D, Zhou H, Zheng T, Yin Y, Lin H (2018) Transcription factor HAT1 is a substrate of SnRK2.3 kinase and negatively regulates ABA synthesis and signaling in Arabidopsis responding to drought. PLoS Genet **14:** e1007336

Templeton GW, Nimick M, Morrice N, Campbell D, Goudreault M, Gingras AC, Takemiya A, Shimazaki K, Moorhead GB (2011) Identification and characterization of AtI-2, an *Arabidopsis* homologue of an ancient protein phosphatase 1 (PP1) regulatory subunit. Biochem J **435:** 73–83

Umezawa T, Sugiyama N, Mizoguchi M, Hayashi S, Myouga F, Yamaguchi-Shinozaki K, Ishihama Y, Hirayama T, Shinozaki K (2009) Type 2C protein phosphatases directly regulate abscisic acid-activated protein kinases in *Arabidopsis*. Proc Natl Acad Sci USA **106:** 17588–17593

Verbinnen I, Ferreira M, Bollen M (2017) Biogenesis and activity regulation of protein phosphatase 1. Biochem Soc Trans **45:** 89–99

Vishwakarma K, Upadhyay N, Kumar N, Yadav G, Singh J, Mishra RK, Kumar V, Verma R, Upadhyay RG, Pandey M, et al (2017) Abscisic acid signaling and abiotic stress tolerance in plants: A review on current knowledge and future prospects. Front Plant Sci **8:** 161

Wang C, Shang JX, Chen QX, Oses-Prieto JA, Bai MY, Yang Y, Yuan M, Zhang YL, Mu CC, Deng Z, et al (2013) Identification of BZR1-interacting proteins as potential components of the brassinosteroid signaling pathway in *Arabidopsis* through tandem affinity purification. Mol Cell Proteomics **12:** 3653–3665

Wang K, He J, Zhao Y, Wu T, Zhou X, Ding Y, Kong L, Wang X, Wang Y, Li J, et al (2018) EAR1 negatively regulates ABA signaling by enhancing 2C protein phosphatase activity. Plant Cell **30:** 815–834

Wang W, Ye R, Xin Y, Fang X, Li C, Shi H, Zhou X, Qi Y (2011) An importin β protein negatively regulates microRNA activity in *Arabidopsis*. Plant Cell **23:** 3565–3576

Wang W, Zhang J, Qin Q, Yue J, Huang B, Xu X, Yan L, Hou S (2014) The six conserved serine/threonine sites of REPRESSOR OF *ga1-3* protein are important for its functionality and stability in gibberellin signaling in *Arabidopsis*. Planta **240:** 763–779

Wang X, Guo C, Peng J, Li C, Wan F, Zhang S, Zhou Y, Yan Y, Qi L, Sun K, et al (2019) ABRE-BINDING FACTORS play a role in the feedback regulation of ABA signaling by mediating rapid ABA induction of ABA co-receptor genes. New Phytol **221:** 341–355

Weith M, Seiler J, van den Boom J, Kracht M, Hulsmann J, Primorac I, Del Pino Garcia J, Kaschani F, Kaiser M, Musacchio A, et al (2018) Ubiquitin-independent disassembly by a p97 AAA-ATPase complex drives PP1 holoenzyme formation. Mol Cell **72:** 766–777

Yan J, Liu Y, Huang X, Li L, Hu Z, Zhang J, Qin Q, Yan L, He K, Wang Y, et al (2019) An unreported NB-LRR protein SUT1 is required for the autoimmune response mediated by type one protein phosphatase 4 mutation (*topp4-1*) in Arabidopsis. Plant J **100:** 357–373

Yang W, Zhang W, Wang X (2017) Post-translational control of ABA signalling: The roles of protein phosphorylation and ubiquitination. Plant Biotechnol J **15:** 4–14

Yoo S-D, Cho Y-H, Sheen J (2007) Arabidopsis mesophyll protoplasts: A versatile cell system for transient gene expression analysis. Nat Protoc **2:** 1565–1572

Yu F, Wu Y, Xie Q (2016) Ubiquitin-proteasome system in ABA signaling: From perception to action. Mol Plant **9:** 21–33

Yue J, Qin Q, Meng S, Jing H, Gou X, Li J, Hou S (2016) TOPP4 regulates the stability of PHYTOCHROME INTERACTING FACTOR5 during photomorphogenesis in Arabidopsis. Plant Physiol **170:** 1381–1397

Zhang J, Hafeez MT, Di D, Wu L, Zhang L (2019) Precise control of ABA signaling through post-translational protein modification. Plant Growth Regul **88:** 99–111

Zheng Y, Schumaker KS, Guo Y (2012) Sumoylation of transcription factor MYB30 by the small ubiquitin-like modifier E3 ligase SIZ1 mediates abscisic acid response in *Arabidopsis thaliana*. Proc Natl Acad Sci USA **109:** 12822–12827

Zhu JK (2016) Abiotic stress signaling and responses in plants. Cell **167:** 313–324

Zong W, Tang N, Yang J, Peng L, Ma S, Xu Y, Li G, Xiong L (2016) Feedback regulation of ABA signaling and biosynthesis by a bZIP transcription factor targets drought-resistance-related genes. Plant Physiol **171:** 2810–2825